



Parameterization of air–sea gas fluxes at extreme wind speeds

Craig McNeil ^{a,*}, Eric D’Asaro ^b

^a *Graduate School of Oceanography, University of Rhode Island, South Ferry Road, Narragansett, RI 02882, USA*

^b *Applied Physics Laboratory and Department of Oceanography, University of Washington, 1013 NE 40th Street, Seattle, WA 98105, USA*

Received 9 November 2005; accepted 17 May 2006

Abstract

Air–sea flux measurements of O₂ and N₂ obtained during Hurricane Frances in September 2004 [D’Asaro, E. A. and McNeil, C. L., 2006. Measurements of air–sea gas exchange at extreme wind speeds. *Journal Marine Systems*, this edition.] using air-deployed neutrally buoyant floats reveal the first evidence of a new regime of air–sea gas transfer occurring at wind speeds in excess of 35 m s⁻¹. In this regime, plumes of bubbles 1 mm and smaller in size are transported down from near the surface of the ocean to greater depths by vertical turbulent currents with speeds up to 20–30 cm s⁻¹. These bubble plumes mostly dissolve before reaching a depth of approximately 20 m as a result of hydrostatic compression. Injection of air into the ocean by this mechanism results in the invasion of gases in proportion to their tropospheric molar gas ratios, and further supersaturation of less soluble gases. A new formulation for air–sea fluxes of weakly soluble gases as a function of wind speed is proposed to extend existing formulations [Woolf, D.K., 1997. Bubbles and their role in gas exchange. In: Liss, P.S., and Duce, R.A., (Eds.), *The Sea Surface and Global Change*. Cambridge University Press, Cambridge, UK, pp. 173–205.] to span the entire natural range of wind speeds over the open ocean, which includes hurricanes. The new formulation has separate contributions to air–sea gas flux from: 1) non-supersaturating near-surface equilibration processes, which include direct transfer associated with the air–sea interface and ventilation associated with surface wave breaking; 2) partial dissolution of bubbles smaller than 1 mm that mix into the ocean via turbulence; and 3) complete dissolution of bubbles of up to 1 mm in size via subduction of bubble plumes. The model can be simplified by combining “surface equilibration” terms that allow exchange of gases into and out of the ocean, and “gas injection” terms that only allow gas to enter the ocean. The model was tested against the Hurricane Frances data set. Although all the model parameters cannot be determined uniquely, some features are clear. The fluxes due to the surface equilibration terms, estimated both from data and from model inversions, increase rapidly at high wind speed but are still far below those predicted using the cubic parameterization of Wanninkhof and McGillis [Wanninkhof, R. and McGillis, W.R., 1999. A cubic relationship between air–sea CO₂ exchange and wind speed. *Geophysical Research Letters*, 26:1889–1892.] at high wind speed. The fluxes due to gas injection terms increase with wind speed even more rapidly, causing bubble injection to dominate at the highest wind speeds.

© 2006 Elsevier B.V. All rights reserved.

Keywords: Air–Sea Exchanges; Hurricanes; Parameterization; Dissolved Gases

1. Introduction

The functional dependence of air–sea gas transfer rates on wind speed has received much attention in the literature, and a large range of dependencies have been proposed, including piecewise linear (Liss and Merlivat,

* Corresponding author.

E-mail address: mcneil@gso.uri.edu (C. McNeil).

1986, or LM-86), quadratic (Wanninkhof, 1992, or W-92), intermediate (Nightingale et al., 2000, or N-2000), and cubic (Wanninkhof and McGillis, 1999, or WM-99). Due to the large range of functionalities that have been proposed to date, it is not clear whether a universal wind speed versus gas transfer relationship really exists. Field measurements of gas transfer rates at wind speeds in excess of 15 m s^{-1} are limited, and only a few measurements exist at wind speeds of up to approximately 20 m s^{-1} , primarily due to the extreme difficulty of sampling under such conditions.

To improve understanding of air–sea gas transfer rates and mechanisms under conditions of extreme wind speed, a field program was conducted during Hurricane Frances using air-deployed gas-sensing floats equipped with O_2 and N_2 sensors (D'Asaro and McNeil, 2006). Three overarching questions of the study are: 1) are any of the existing parameterizations excluded at extreme wind speeds?; 2) empirically, what functional dependence of air–sea gas transfer rates on wind speed best describes air–sea gas transfer rates over the entire natural range of wind speeds?; and 3) what are the dominant physical processes that control air–sea gas exchange at extreme wind speeds? To address these questions, a new model of air–sea gas transfer was formulated and calibrated against the field data. Remaining critical knowledge gaps are identified, where possible.

2. Current understanding of air–sea gas transfer

The model of air–sea gas flux developed in this paper is concerned chiefly with the transfer of weakly soluble gases, such as O_2 , N_2 , and the noble gases. Implications for the transfer of CO_2 , a much more soluble gas, will be discussed in Section 4.11.

2.1. Surface equilibration processes

Gas exchange across a stagnant air–water interface is controlled by molecular diffusion. A thin boundary layer of equilibrated water, typically a few hundred microns in depth, develops at the surface of an initially degassed water mass within a few seconds after exposure. The dissolved gas concentration, c_a , at the air–water interface can be calculated using Henry's Law, $c_a = S_H p_a$, where S_H is the gas solubility coefficient (either $\text{mol kg}^{-1} \text{ atm}^{-1}$ or $\text{mol l}^{-1} \text{ atm}^{-1}$), which varies with seawater temperature and salinity, and p_a is the partial pressure of the gas in the atmosphere (Garcia and Gordon, 1992; Hamme and Emerson, 2004). Gases will penetrate deeper into the water as the boundary layer grows, but at a decelerating rate, as described by $h(t) = (Dt)^{-1/2}$, where h is the depth

of the layer, t is time, and D is the molecular diffusivity of the gas in seawater. The air-saturated boundary layer will inhibit further exchange of gas between the bulk fluid and the atmosphere, thereby decreasing the net air–water flux over time. Regardless of the saturation level of the bulk fluid, the net air–water flux will diminish in less than a minute. If net heat fluxes are non-zero, a thermal boundary layer will also develop. Because gas solubility depends on water temperature, this will affect c_a . Typically, a 'cool skin' develops over the ocean due to evaporation and infrared heat loss.

The sea surface cannot become truly stagnant, though gas exchange may be severely limited in very calm conditions and in the presence of strong surfactant slicks. Generally, wind and waves create turbulence and eddies that continuously erode the surface microlayer by various surface-renewal and eddy-divergence mechanisms, resulting in enhanced air–sea gas transfer rates. Surface microbreaking, which disturbs the surface but does not create bubbles, has also been proposed as a ubiquitous process that enhances air–sea gas transfer rates. Under more energetic conditions, larger-scale eddies and convergences in the bulk fluid will replenish the surface water with fluid from the bulk. Active breaking waves create localized patches at the sea surface with low impedance to gas transfer. The turbulent patch receives energy for mixing from the bubbles released from the submerged bubble plume during its senescence period.

Air–sea gas exchange associated with processes that act at the sea surface by disturbing the boundary layer can be described collectively by a gas transfer rate, K_s (m s^{-1}), where the subscript 's' indicates 'surface'. The corresponding air–sea gas flux, Q_s , is:

$$Q_s = K_s(c_w - c_a), \quad (1)$$

where c_w is the concentration of the gas in the bulk fluid.

Unlike the air–sea interface, which relies on erosion from below to renew the boundary layer, a bubble has a 'self-cleaning' mechanism that replenishes its boundary layer with fluid from the bulk as it rises through the water. This provides an efficient way to aerate the seawater. A bubble with a radius greater than approximately $100 \mu\text{m}$ that is within 10 cm of the sea surface has an internal pressure within 1% of atmospheric pressure. A plume of such bubbles can be considered a submerged extension of the air–sea interface, and therefore the fluid in the plume will rapidly equilibrate to near 100% of equilibrium saturation with respect to the atmosphere. Under these conditions, the water in the plume cannot supersaturate by more than 1%. Large bubbles are quickly released back to the atmosphere and thus have little time to transfer weakly

soluble gases. The rise speed of a 1-mm bubble is on the order of 0.2 m s^{-1} . Smaller bubbles rise more slowly, have greater residence times in the water, and therefore more fully equilibrate, but they have smaller surface areas available for gas transfer. In general, wave breaking-induced bubble plumes near the surface will not supersaturate the water significantly, and therefore this process can be considered to enhance K_s . This point is discussed in more detail in Section 4.4. The importance of this process to the air–sea exchange of CO_2 was pointed out by Keeling (1993).

Surface tension creates significant excess internal pressure in bubbles with radii smaller than approximately $20 \mu\text{m}$ in seawater. Thus, bubbles with radii greater than approximately $20 \mu\text{m}$ near the surface of the ocean act to equilibrate the ocean to 100% of equilibrium saturation with respect to the atmosphere. These bubbles can be suspended in near-surface turbulence for many minutes before bursting at the surface or dissolving. They also act to enhance K_s .

2.2. Partial dissolution of bubbles

Turbulence, generated by breaking waves and vertical shear in horizontal currents, mixes bubbles from the sea surface to a characteristic depth that depends on the bubble's rise velocity according to $Z = A_v/U$, where A_v is the vertical eddy diffusivity and U is the rise speed of the bubble. Vertical turbulent diffusion and advection of bubbles, such as that which occurs in Langmuir circulation, will transport small bubbles to increased depth, where they partially dissolve before resurfacing. Some fraction of these bubbles may also completely dissolve.

Consider a small air bubble that is entrained in a turbulent plume of water moving at a constant speed deeper into the oceanic mixed layer. As the bubble moves deeper, the internal pressure increases due to compression by hydrostatic forces. At any particular depth, if the bulk water in the plume is undersaturated with respect to the instantaneous equilibrium solubility at the bubble's surface, air will be forced into solution according to Henry's Law and the bubble will begin to dissolve. The equilibrium concentration at the bubble's surface increases by a factor of two between 0–10 m depth. As the bubble is compressed further, its rise speed decreases. The loss of air from the bubble to the water further reduces its volume, which in turn further decreases its rise speed. In this way, a bubble may completely dissolve, even if the entraining fluid parcel slows down. If the fluid parcel stops at a particular depth, the bubble will naturally rise toward the sea surface. The bubble may continue to dissolve on its way up if the water is undersaturated; it may dissolve

completely before it reaches the surface, or it may strip dissolved gases from the water above a critical depth. Note that bubbles can strip dissolved gases from the water even if the bulk water is supersaturated with respect to the atmosphere. Partial bubble dissolution within submerged and dynamic bubble clouds is a complex problem (see discussions in Asher et al., 1996; Woolf, 1997).

A further complication associated with bubbles arises specifically for N_2 and O_2 , because the net flux of one gas from a bubble plume depends on the dissolved concentration of the other gas. This coupling arises because the total pressure inside a bubble, which affects the size and hence rise speed and dissolution rate of the bubble, depends primarily on the sum of the partial pressures of dissolved N_2 and O_2 . Woolf and Thorpe (1991) modeled gas transfer from turbulent bubble plumes within idealized Langmuir circulation cells using Monte Carlo simulations. Their model revealed equilibrium steady state supersaturation levels for different gases, variable Langmuir downwelling velocities, variable initial bubble size spectra, and other factors. They reported simplified expressions for the equilibrium fractional supersaturation level, Δ_i , for any gas denoted by subscript 'i', as a quadratic dependence on wind speed, $\Delta_i = 0.01 \times (U_{10}/U_i)^2$, where U_{10} is the steady wind speed at 10 m height, $U_{\text{N}_2} = 7.2 \text{ m s}^{-1}$ for nitrogen, and $U_{\text{O}_2} = 9.0 \text{ m s}^{-1}$ for oxygen. At any particular wind speed, Δ is larger for less soluble gases. This is easily explained by considering the effects of the two gases on gas saturation levels. For the less soluble gas, the fractional increase in dissolved gas concentration due to dissolution of the bubble will be large, and vice versa. Thus, the saturation level increase will be greater for an insoluble gas than a soluble gas.

Woolf (1997) proposed the following equation to incorporate the role of small bubbles in supersaturating water:

$$Q_{\text{net}} = (K_o + K_b)[c_w - c_a(1 + \Delta)], \quad (2)$$

where Q_{net} is the net air–sea gas flux, K_o is the gas transfer rate associated with direct non-bubble-mediated transfer mechanisms (similar but not identical to K_s described above), and K_b is the gas transfer rate associated with bubbles in general. The equation leads to a steady state supersaturation of any gas at any constant wind speed.

2.3. Complete bubble dissolution

Spitzer and Jenkins (1989) were likely the first to include a separate term to describe the complete

dissolution of bubbles, or bubble ‘injection,’ in a parameterization of air–sea gas fluxes. They introduced the term to explain inert gas saturation levels in the NW Atlantic. Recently, Hamme and Emerson (2002) interpreted dissolved inert gas profiles from the Atlantic and Pacific using a quasi steady state model of water mass formation. They assumed that the total air–sea gas transfer rate could be divided into two terms: one associated with all processes that equilibrate ocean surface waters towards 100% equilibrium saturation with respect to the atmosphere, similar in principal to the K_s term described above; and a second term that represents complete bubble-injection processes only, which they denoted by K_i . By matching model results to the data, they estimated that the ratio K_i/K_s varied from approximately 0.1 to 0.3.

For any gas, the total air–sea flux associated with complete bubble injection can be written as:

$$Q_i = -V\chi_i, \quad (3)$$

where V is the number of moles of air per unit surface area of the ocean and per unit time that enters the ocean as bubbles and dissolves completely, and χ_i is the dry air mole fraction of the gas in the atmosphere. It is noted that the Woolf and Thorpe model (1991) implicitly contains a Q_i term, though its dependence on U_{10} was not reported.

3. Observations during Hurricane Frances

The air–sea fluxes of O_2 and N_2 obtained during Hurricane Frances and used in Section 4 of this paper are described in detail by D'Asaro and McNeil (2006). Two neutrally buoyant Lagrangian floats (D'Asaro, 2003, 2004) equipped with dissolved gas sensors (McNeil et al., in press) were air deployed into the path of Hurricane Frances on 31 August, 2004. The floats accurately followed the vertical motions of water parcels in the 20–40 m thick surface mixing layer during the passage of the storm while measuring temperature, salinity, pressure, and the dissolved O_2 and N_2 concentrations of these parcels. Air–sea fluxes of N_2 and O_2 were estimated from these measurements using several nearly independent methods. Upper ocean budgets, based on a vertical mixing model calibrated to temperature, were used to derive budget fluxes of N_2 and O_2 . Eddy covariance fluxes of $O_2 = \langle wO_2' \rangle$ were computed from simultaneous measurements of vertical velocity w and perturbations of O_2 . Surface fluxes were computed from the integrated deficit of O_2 in the upper two meters and a residence time of water in this layer computed from the float trajectories. At the height of

the storm, the data clearly indicate that complete bubble dissolution (see Section 2.3) is the dominant process and that the dissolution happens at about 10 m depth. Note that the budget and covariance methods give the total air–sea flux, while the surface fluxes measure only that part of the flux that removes gas from the upper two meters and therefore does not include the contribution of bubble dissolution at greater depths. Wind speeds at the floats were estimated by interpolating daily averaged maps of the hurricane winds (Powell et al., 1998) to the times and positions of the floats. This process ignores known higher frequency changes in the winds potentially causing errors in the wind timing of a few hours.

Fig. 1a shows the wind speed dependence of the budget-derived N_2 and O_2 fluxes (envelope of the color shaded regions, O_2 in red and N_2 in blue). At the highest winds, the gas flux ratio is similar to that of standard tropospheric air (approximately 3.73:1). This provides compelling evidence that the air–sea gas fluxes were associated mostly with complete bubble-injection processes. The structure of the covariance profiles and examination of the O_2 variations along the float trajectories provides additional evidence (D'Asaro and McNeil, 2006). Another feature of the observations is a hysteresis in the gas fluxes with wind speed. Fluxes were higher on the rising wind than the falling wind, or, equivalently, the peak in winds occurred later than the peak in fluxes. One explanation is that the bubble injection flux depends on wave breaking rather than wind and that wave breaking is stronger during rising winds. This interpretation indicates that gas fluxes at hurricane-force winds cannot be parameterized by wind speed alone. It is also possible, however, that a timing error in the wind speed estimates exists or a timing error is introduced by the 1-D modeling approach. Here, it is assumed that this hysteresis is due to an error. Thus, Fig. 1a also shows ‘wind-shifted’ budget-derived fluxes (thick lines, O_2 in red and N_2 in blue) obtained by advancing the gas fluxes relative to the winds by 100 min. This aligns the peak in the gas fluxes to the peak winds of the hurricane. The wind-shifted fluxes will also be used in the model-data comparisons in Section 4 of this paper.

Also shown in Fig. 1a are six discrete estimates of the near surface O_2 evasion flux. The two medium size red dots are surface flux estimates corresponding to wind speeds of approximately 37 and 50 $m s^{-1}$. The four small red dots at lower wind speeds ranging from approximately 14–27 $m s^{-1}$ are covariance-derived estimates. Before, and especially after, the peak of the storm, the bulk and covariance-derived O_2 fluxes are out of the ocean, consistent with downgradient flux from the supersaturated ocean. This implies that during this

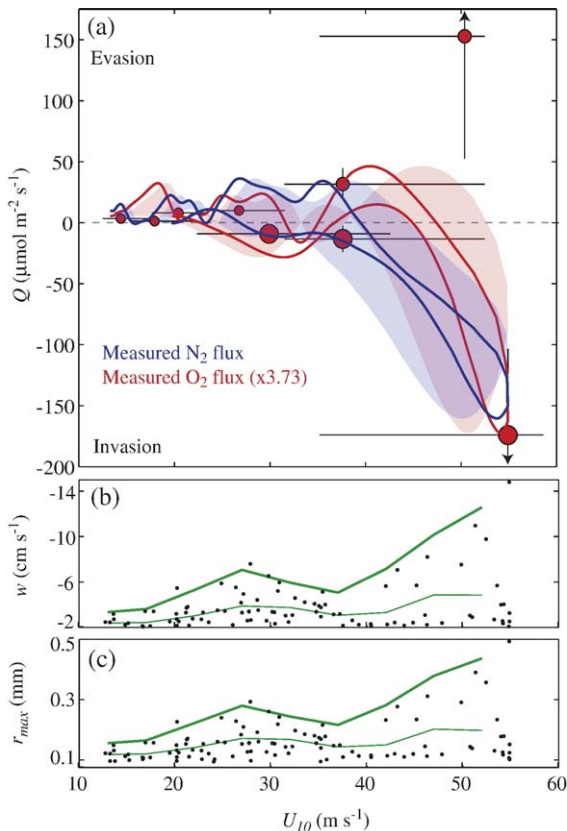


Fig. 1. Summary of Hurricane Frances measurements, showing: (a) N_2 budget-derived fluxes (blue thick lines) and O_2 fluxes (red thick lines) for the case of wind speed at 10 m height (U_{10}) delayed with respect to gas fluxes by 100 min, and corresponding fluxes for the case of no delay in wind speed (envelope of the shaded regions); O_2 covariance-derived fluxes during periods of evasion (small red dots) and invasion (large red dots) with error bars (black lines) derived from float statistics; and near surface O_2 deficit-derived estimates (medium size red dots); all O_2 fluxes are amplified by a factor of 3.73, the molar ratio for N_2/O_2 in standard dry tropospheric air; loss of gas from the ocean to the atmosphere, or evasion, is defined for positive fluxes and vice versa for invasion; (b) statistics of the downward-flowing turbulent current velocity (w) within 2.5 m of the sea surface inferred from float movement; shown are means (thin solid green line), and means plus twice the standard deviation (thick solid green line); (c) maximum radii of bubbles (r_{max}) that can be transported with the turbulent currents, estimated using the terminal rise velocity relationship of Clift et al. (1978); see (b) for description of line types.

period, bubble supersaturation effects are insignificant. Fig. 1b shows statistically based estimates of the float's downward-moving vertical velocity (w) within 2.5 m of the sea surface. The dots show all downward going velocities with magnitude greater than 2 cm s^{-1} ; the line shows the average and the average plus 2 standard deviations of these points in velocity bins. Assuming the floats follow the water motions, these statistics are representative of the downward-flowing larger scale

turbulent currents emanating from near the sea surface. The mean and variance of w increase with wind speed; maximum velocities of just over -14 cm s^{-1} were observed (Fig. 1b). Such strong vertical currents will transport not only the floats, but also bubbles away from the near surface to depth. An estimate of the maximum radii of bubbles (r_{max}) that could possibly be carried down into the ocean by such descending turbulent currents, made by comparing w to the bubble rise velocity relationship of Clift et al. (1978), is shown in Fig. 1c. Bubbles with radii smaller than r_{max} would compress under increasing hydrostatic pressure and therefore dissolve. This analysis shows that at the peak of the hurricane, bubbles of size up to 1 mm in diameter could be transported to depth by turbulent currents. For these calculations, plume effects, such as the bubble's effect on the seawater density and aggregation and break-up of bubbles, are assumed to be small. This assumption will be problematic for dense plumes. These calculations are used in a simple formulation of bubble injection described in Section 4.

Taken together, the observations made during Hurricane Frances (D'Asaro and McNeil, 2006) indicate a previously unobserved regime of bubble-mediated air–sea gas exchange in which plumes of bubbles with sizes up to a millimeter are transported from the near surface ocean to depths of more than 10–20 m by energetic downward flowing turbulent currents. The bubbles are compressed by hydrostatic pressure and dissolve completely. This process acts to supersaturate the mixed layer waters and flux air into the ocean. Upward flowing turbulent currents return supersaturated waters to the surface where it can degas back to the atmosphere (see Fig. 15, D'Asaro and McNeil, 2006). These insights into the processes which act to exchange gases between the atmosphere and ocean at high to extreme wind speeds were used to develop a new parameterization of air–sea gas exchange suitable for describing transfer of weakly soluble gases over a full range of wind speeds. This new model is described next.

4. Model

4.1. Formulation

The new parameterization of air–sea gas transfer is:

$$Q_{\text{net}} = Q_s + Q_b + Q_i = K_s(c_w - c_a) + K_b[c_w - c_a(1 + \delta)] - V\chi, \quad (4)$$

where Q_s is calculated from Eq. (1) and represents surface equilibration processes only; $Q_b = K_b[c_w - c_a(1 + \delta)]$

represents the air–sea flux associated mostly with partial dissolution of bubbles much less than 1 mm in size that are within bubble plumes, physically maintained by vertical eddy mixing and advection and a balance of bubble dissolution and growth; and Q_i is calculated from Eq. (3) and represents the flux from complete dissolution of bubbles 1 mm or less in size that are transported deep into the ocean mixed layer by strong turbulent currents that may occur, for example, at the convergence zones of large-scale, actively forced eddies. Here, K_s and K_b assume a standard $Sc^{-1/2}$ dependence under conditions of strong turbulence (see, for example, Clift et al., 1978; Wanninkhof, 1992). Note that Q_i does not depend on gas diffusivity, because the entire plume is assumed to dissolve.

The δ term in Eq. (4) is similar to Δ in Eq. (2) and can likewise be expected to depend on the gas solubility, diffusivity, and saturation level of the other major constituent gas (*i.e.*, N_2 or O_2) as described by Woolf (1997). If the contribution of complete dissolution of bubbles to Δ is defined to be γ , to a first order approximation it follows that $\gamma = \Delta - \delta$. The equivalent air–sea gas flux required to maintain the supersaturation γ can then be calculated and incorporated directly into the term Q_i . An analysis of this problem would require simulations of bubbles and large eddies in the upper ocean over a full range of wind speeds. However, the predictive skill of such models will depend largely on the accuracy of the physics of the mixed layer.

There is one fundamental difference between Eq. (4), with $V=0$, and Eq. (2). When Eq. (2) is used with $K_b=0$, a steady state supersaturation of the oceanic mixed layer is predicted at any steady wind speed. This prediction is inconsistent with the specification that no supersaturating processes occur ($K_b=0$). By separating the terms in Eq. (2) into two components as in Eq. (4), this problem is rectified. This point will be discussed again in Section 4.2.

Fundamentally, Eq. (4) has four variables: K_s , K_b , δ , and V , each of which likely depends on wind speed, wave breaking, and the nature of the turbulence in the upper ocean in some unknown way. If each term is assumed to depend solely on wind speed, and each gas (O_2 and N_2) can be described by one equation, then the system of equations is underdetermined (2 equations and 4 variables). The model can be simplified, however, by re-writing it as:

$$\begin{aligned} Q_{\text{net}} &= Q_{ST} + Q_{BT} \\ &= K_T(c_w - c_a) - (K_b \delta S_H + V)\chi, \\ &= K_T(c_w - c_a) - V_T \chi \end{aligned} \quad (5)$$

where Q_{ST} is the total flux associated with all surface equilibration processes, the total gas ‘piston velocity’ associated with near surface processes is $K_T = K_s + K_b$, and Q_{BT} is the total invasion flux associated with all bubble-

mediated supersaturating processes. By considering the term $K_b \delta S_H$ as a single variable, Eq. (5) has 3 variables (K_T , $K_b \delta S_H$, V), each of which is assumed to be a function of wind speed. By grouping the terms further and defining the term $V_T = (K_b \delta S_H + V)$ as a new variable, Eq. (5) in its simplest form has 2 variables (K_T , V_T). In this last formulation, however, V_T may be different for O_2 and N_2 , so the number of variables has not really been reduced.

4.2. Idealized model response to a step change in wind speed

To further investigate the difference between Eqs. (2) and (4) with $V=0$, the response of the upper ocean to a step change in wind speed was modeled using both equations. For simplicity, it was assumed that no entrainment, temperature, salinity, or air pressure changes occurred. A value of $c_a = 370 \mu\text{mol kg}^{-1}$ for N_2 was used, and the mixed layer was assumed to be initially supersaturated and 80 m deep. The following values were chosen for the N_2 transfer rates: $K_o = K_s = 0.375 \text{ m h}^{-1}$ and $K_b = 0.219 \text{ m h}^{-1}$ at $U_{10} = 10 \text{ m s}^{-1}$, and $K_o = K_s = 1.5 \text{ m h}^{-1}$ and $K_b = 3.5 \text{ m h}^{-1}$ at $U_{10} = 40 \text{ m s}^{-1}$. In addition, δ was assumed equal to Δ , where $\Delta = 7.2 \text{ m s}^{-1}$ for N_2 (Woolf and Thorpe, 1991).

The model results are shown in Fig. 2. In the case of no surface fluxes (*i.e.*, $K_o=0$ in Eq. (2), and $K_s=V=0$ in Eq. (4)), both equations produced the same result, and the evasion of gases from the ocean’s mixed layer before and after the step increase in wind speed is associated, conceptually, with the stripping of gases in the water column and their release back into the atmosphere by the surfacing of small submerged bubbles. For the limiting case of no deeply submerged bubbles (*i.e.*, $K_b=0$ in Eq. (2), and $K_b=V=0$ in Eq. (4)), both equations produce very different results. Eq. (2) produces a supersaturated ocean during the idealized storm, which should not happen in the absence of deeply submerged bubbles. This is an artifact of how the K_o and K_b terms are represented in Eq. (2). This artifact can be removed by separating the K_o and K_b terms, similar to Eq. (4). Eq. (4) correctly predicts that the ocean will equilibrate to the atmospheric equilibrium values during the storm in the absence of deeply submerged bubbles. Also note that the steady state supersaturation levels (Fig. 2, thick solid lines around day 10) are less for Eq. (4) than for Eq. (2). The equilibrium steady state supersaturation levels are related algebraically by $\delta = \Delta(1 - K_s/K_b)$.

4.3. Low wind speed estimates of K_T

The first assumption used is that all model coefficients are functions of the time-lagged wind. The second

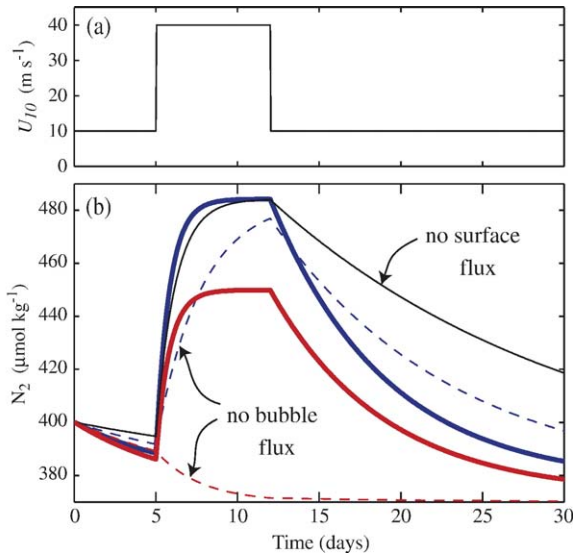


Fig. 2. Modeled changes in oceanic mixed layer dissolved N_2 concentration in response to a step change in wind speed, showing: (a) wind speed at 10 m height, U_{10} ; and (b) dissolved N_2 concentration using Eq. (2) (thick blue line), and Eq. (4) with $V=0$ (thick red line). Also shown in (b) are the results for the limiting cases of $K_0=0$ in Eq. (2) (thin black line), and $K_s=0$, $V=0$ and $\delta=\Delta$ in Eq. (4) (same thin black line). Also shown are the results for the limiting cases of $K_b=0$ in Eq. (2) (thin dashed blue line) and the associated unrealistic equilibrium supersaturation during the storm, and $K_b=0$ and $V=0$ in Eq. (4) (thin dashed red line) and the realistic equilibration to 100% air-saturation.

assumption used is that $V_T=0$ for $U_{10}<27\text{ m s}^{-1}$. The usual formulation of air–sea flux, *i.e.*, Eq. (1), uses this second assumption, and our fluxes qualitatively follow Eq. (1), *i.e.*, gases were lost from the supersaturated ocean at $U_{10}<27\text{ m s}^{-1}$. It is therefore plausible that Eq. (1) remains nearly valid, and V_T can be neglected for $U_{10}<27\text{ m s}^{-1}$ during Hurricane Frances. At higher wind speeds, the observed air–sea gas flux reverses sign. The data then clearly indicate the importance of bubble injection, so V_T cannot be neglected. Accordingly, the discrete O_2 covariance-derived flux estimates (*i.e.*, Q_{ST} ; see Fig. 1a, small red dots, or Table 2 — Covariance Fluxes, from D'Asaro and McNeil, 2006) were used to estimate K_T for $U_{10}<27\text{ m s}^{-1}$. These are shown in Fig. 3 (small red dots).

4.4. High wind speed estimates of K_T

The generally 8–9% supersaturated waters of the near surface layer (0–2.5 m depth) at $U_{10}=37.6\text{ m s}^{-1}$ and $U_{10}=50.4\text{ m s}^{-1}$ were observed (see Table 2 — Surface Fluxes, D'Asaro and McNeil, 2006) to be reduced in O_2 relative to the underlying well mixed

waters, as discussed in Section 3. Because the observations indicated that complete bubble injection occurs in the depth range 10–20 m, well below this O_2 -deficit surface layer, it is assumed that $V=0$ for this layer. Also, partial bubble dissolution can be expected to occur mostly at depths greater than 0.8–0.9 m, the depth range at which hydrostatic pressure equals the excess gas tension associated with the supersaturation, and so it is reasonable to assume that $K_b \delta S_H$ does not contribute significantly. Both arguments support the use of $V_T=0$ for this layer. Accordingly, the two surface O_2 -flux estimates (*i.e.*, Q_{ST} ; see Fig. 1a, medium size red dots) are used to estimate K_T for $U_{10}>27\text{ m s}^{-1}$. These estimates are shown in Fig. 3 (medium size red dots).

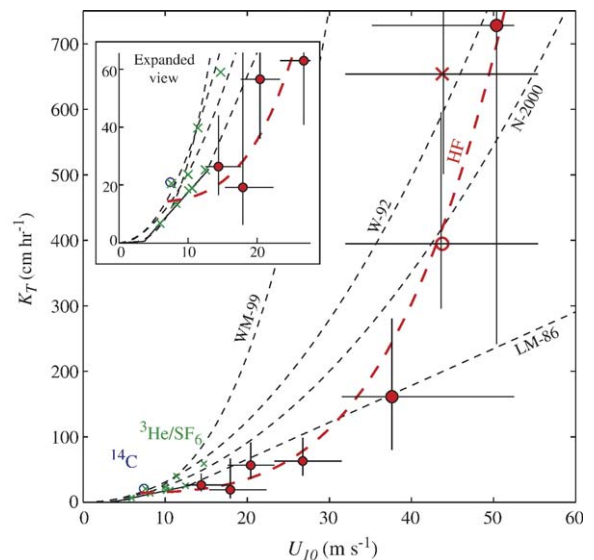


Fig. 3. Dependence of air–sea gas transfer rate (K_T , normalized to $Sc=660$) on wind speed at 10 m height (U_{10}) from: Liss and Merlivat (1986), LM-86; Wanninkhof (1992), W-92; Wanninkhof and McGillis (1999), WM-99; and Nightingale et al. (2000), N-2000 (thin black dashed lines). Also shown are the global bomb carbon (^{14}C , blue open circle) data point from Broecker et al. (1985) and reanalyzed dual-tracer measurements ($^3He/SF_6$, small green crosses) from four North Sea experiments as described in Nightingale et al. (2000). Data-derived estimates of K_T for Hurricane Frances were derived from covariance-derived O_2 fluxes (small red dots) and near surface O_2 deficit-derived fluxes (medium red dots; see Fig. 2a for corresponding fluxes) calculated assuming no bubble supersaturation effects; a power-law regression fit (thick long dashed red line, marked HF) through the six discrete K_T estimates and constrained by ^{14}C data point is shown. Inverse model derived-estimates of K_T are shown as a mean value (red circle) and maximum value (large red cross), derived using Eq. (6) and budget-derived net gas fluxes delayed with respect to U_{10} by 100 min; only positive values of the inverse solution for $U_{10}>30\text{ m s}^{-1}$ were used in these calculations, and errors bars were calculated using $\pm 25\%$ errors in gas fluxes. The insert (top left) shows an expanded view of the low wind speed data.

4.5. Regression fit of K_T versus U_{10}

A least-squares power law fit to all six discrete K_T estimates is shown in Fig. 3 (red dashed line, marked HF) and specified by $K_T = a + b \times (U_{10})^c$ in units of cm h^{-1} , with $a = 14$ (fixed), $b = 0.0002925$ ($-0.001215, 0.0018$), and $c = 3.742$ ($2.415, 5.069$); the numbers in parenthesis are the 95% confidence bounds, and $r^2 = 0.9752$. The low wind speed constraint was imposed to match the expected value for short-term winds (see Wanninkhof, 1992) appropriate for ^{14}C using N-2000.

4.6. Inverse solution, obtained by eliminating V_T

Additional progress can be made by using the most simplified form of Eq. (5) with the assumption that V_T is the same for O_2 and N_2 at high wind speeds. In this case, there are two equations, one each for the net fluxes of O_2 (i.e., $Q_{\text{net}}^{\text{O}_2}$) and N_2 (i.e., $Q_{\text{net}}^{\text{N}_2}$), and two variables (i.e., K_T and V_T). Solving these two equations by eliminating V_T results in an ‘inverse’ solution for K_T as follows:

$$K_T(\text{Sc} = 660) = \frac{\chi^{\text{N}_2} Q_{\text{net}}^{\text{O}_2} - \chi^{\text{O}_2} Q_{\text{net}}^{\text{N}_2}}{\chi^{\text{N}_2} \left(\frac{\text{Sc}^{\text{O}_2}}{660}\right)^{-1/2} (c_w^{\text{O}_2} - c_a^{\text{O}_2}) - \chi^{\text{O}_2} \left(\frac{\text{Sc}^{\text{N}_2}}{660}\right)^{-1/2} (c_w^{\text{N}_2} - c_a^{\text{N}_2})} \quad (6)$$

with $\chi^{\text{O}_2} = 0.20946$ and $\chi^{\text{N}_2} = 0.78084$, following standard tropospheric ratios. Note that the inverse solution goes to zero when the numerator is zero, i.e., when the observed net gas flux ratio ($Q_{\text{net}}^{\text{O}_2}/Q_{\text{net}}^{\text{N}_2}$) equals the tropospheric ratio. This occurs at the peak winds of the hurricane. Also note that the inverse solution has a singularity when the denominator equals zero, i.e., when the surface flux ratio ($Q_s^{\text{O}_2}/Q_s^{\text{N}_2}$) equals zero.

The inverse solution of K_T described by Eq. (6) was calculated using the wind-shifted budget-derived gas fluxes at $U_{10} > 30 \text{ m s}^{-1}$. The mean $K_T(\text{Sc}=660)$ was 394.8 cm h^{-1} , with an uncertainty range of $300\text{--}600 \text{ cm h}^{-1}$ at a mean $U_{10} = 43.8 \text{ m s}^{-1}$. The maximum value of $K_T(\text{Sc}=660)$ was 653.9 cm h^{-1} , with an uncertainty range of $500\text{--}800 \text{ cm h}^{-1}$. Because negative values of K_T produced by Eq. (6) are unrealistic, these values were not used in these calculations. Uncertainty in the estimates were calculated using $\pm 25\%$ error in $Q_{\text{net}}^{\text{O}_2}$ and $Q_{\text{net}}^{\text{N}_2}$. Fig. 3 shows the mean value (red circle) and maximum value (red cross). The mean value agrees well with the data-derived estimates (HF line). Using the mean K_T estimate from the inverse model and the observed O_2 saturation levels, we can compare the calculated O_2 fluxes (i.e., Q_{ST}) to those estimates

derived using the O_2 -deficit method. Because the transfer rates are comparable, the flux estimates are also comparable: the O_2 -deficit fluxes are $8.5 \mu\text{mol m}^{-2} \text{ s}^{-1}$ at $U_{10} = 37.6 \text{ m s}^{-1}$, and $41.0 \mu\text{mol m}^{-2} \text{ s}^{-1}$ at $U_{10} = 50.4 \text{ m s}^{-1}$, with a mean of $26.3 \mu\text{mol m}^{-2} \text{ s}^{-1}$ at a mean $U_{10} = 44.0 \text{ m s}^{-1}$ (by linear interpolation); the inverse model-derived estimate using the mean value of $K_T = 394.8 \text{ cm h}^{-1}$ at a mean $U_{10} = 43.8 \text{ m s}^{-1}$ provides a mean $Q_{\text{ST}}^{\text{O}_2} = 22.3 \mu\text{mol m}^{-2} \text{ s}^{-1}$. Both estimates of $Q_{\text{ST}}^{\text{O}_2}$ are well within errors and agree to 17%. This agreement provides confidence in the K_T estimates shown by the HF line in Fig. 3 and suggests that the assumption that V_T is the same for O_2 and N_2 at high wind speeds, i.e., that bubble injection of air dominates, is approximately correct.

4.7. Wind speed dependence of Q_{BT}

In Section 4.6 it was shown that the inverse solution to K_T approximately agreed with the HF fit. Using the HF parameterization of $K_T(U_{10})$, and the wind shifted budget-derived $Q_{\text{net}}^{\text{O}_2}$, Eq. (5) can be solved for $Q_{\text{BT}}^{\text{O}_2} = Q_{\text{net}}^{\text{O}_2} - Q_{\text{ST}}^{\text{O}_2}$, and $Q_{\text{BT}}^{\text{N}_2} = Q_{\text{net}}^{\text{N}_2} - Q_{\text{ST}}^{\text{N}_2}$. These results are

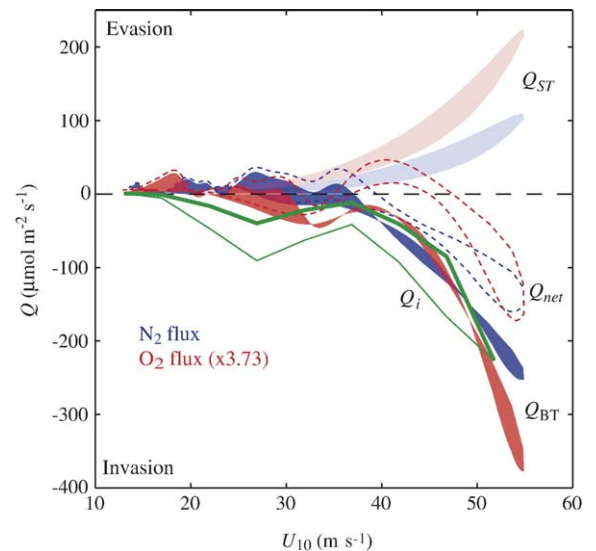


Fig. 4. Modeled air–sea gas fluxes (Q) versus wind speed at 10 m height (U_{10}), calculated using Eq. (5) and wind-shifted budget-derived fluxes, $Q_{\text{net}}^{\text{O}_2}$ (red dashed line) and $Q_{\text{net}}^{\text{N}_2}$ (blue dashed line). Modeled $Q_{\text{ST}}^{\text{O}_2}$ (light red shading) and $Q_{\text{ST}}^{\text{N}_2}$ (light blue shading) use K_T derived from the Hurricane Frances measurements (see heavy dashed red line marked HF in Fig. 3). Calculated $Q_{\text{BT}}^{\text{O}_2}$ (heavy red shading) and $Q_{\text{BT}}^{\text{N}_2}$ (heavy blue shading) are shown. Also shown are modeled Q_i , obtained by integrating over an assumed bubble spectra $n(r)dr \sim r^{-b}$ and scaled in amplitude to match Q_{ST} , for the cases of $b=2$ (thick solid green line) and $b=4$ (thin solid green line). All O_2 fluxes (red lines and shading) are amplified by a factor of 3.73.

shown in Fig. 4. The calculated Q_{BT} show a rapid increase at $U_{10} > 35 \text{ m s}^{-1}$, in accordance with the assumption described in Section 4.3 about the basic functional dependency of $V_T = Q_{BT}/\chi$. A least-squares power law fit to $Q_{BT}^{Air} = Q_{BT}^{N_2} + Q_{BT}^{O_2}$ was calculated and is specified by $Q_{BT}^{Air} = b \times (U_{10})^c$ in units of $\mu\text{mol}(\text{Air}) \text{ m}^{-2} \text{ s}^{-1}$, with $b = -3.282 \times 10^{-9}$ ($-4.027 \times 10^{-9}, -2.537 \times 10^{-9}$), $c = 6.35$ (6.293, 6.407); the numbers in parenthesis are the 95% confidence bounds, and $r^2 = 0.9711$.

4.8. Model results for $V=0$

The model was run for $V=0$. There are many options for the prescription of K_b . For this model run, $K_T = K_s + K_b$ was specified by the line fit HF (see Fig. 3) and K_s was set equal to K_b . This amounts to sharing equally the total gas transfer rate between the surface and partial bubble dissolution processes. Also, δ was specified according to Woolf and Thorpe (1991), with $\delta = \Delta$ (see Eq. (2)), where $U_{O_2} = 9.0 \text{ m s}^{-1}$ and $U_{N_2} = 7.2 \text{ m s}^{-1}$. The results are shown in Fig. 5. The results are similar to those shown in Fig. 4, except the surface fluxes, Q_s , are reduced by a factor of approximately two due to the

sharing of the gas transfer rate with the bubble flux, Q_b . As discussed previously, there is great uncertainty in the model parameters δ , and therefore it is easy to obtain reasonably good fits between model and data for different sets of δ and K_b (with the exception of the gas flux ratio, as discussed below). Because both parameters are expected to have strong non-linear dependence on wind speed, the model results are sensitive to the choice of the coefficients. Hence, it is not a particularly useful exercise at this stage to explore the model further for the case $V=0$ because experimental constraints are poor and non-existent for $U_{10} > 20 \text{ m s}^{-1}$. The important point is that models with either $V=0$ or $K_b=0$ can be tuned to fit the Hurricane Frances data with roughly equal skill.

4.9. Modeled gas flux ratio

At $U_{10} > 40 \text{ m s}^{-1}$, the gas flux ratio $Q_{BT}^{O_2}/Q_{BT}^{N_2}$ agreed with the tropospheric molar gas ratio to within approximately 35%. Also, it was found that $Q_{BT}/Q_{ST} > 1$ at $U_{10} > 37 \text{ m s}^{-1}$. It was not possible to make a reliable estimate at the lower winds speeds because of the noise in the bulk-flux estimates. In addition, we have not yet been able to model accurately the observed gas flux ratio $Q_{net}^{O_2}/Q_{net}^{N_2}$ at both high and low winds speeds; this needs further investigation.

4.10. Bubble injection flux

The estimates of r_{max} shown in Fig. 1c were used to estimate the total volume flux of bubbles associated with fast downward flowing plumes as follows. First, a bubble size spectra of the following form is assumed: $n(r)dr \sim r^{-b}$, where $n(r)$ is the number of bubbles per unit volume of water per unit radius r and per unit radius increment dr . Typically, b is found to decrease with increasing depth, varying from the sea surface to depths of several meters over the range $b = 1-4$, hence bubble plumes contain more small bubbles than large bubbles (see the literature review in Woolf, 1997). The total void fraction associated with the bubble plume is found by integrating over the bubble spectra to obtain an estimate of the total volume of air contained in the bubble plume as follows:

$$v_f = \frac{4\pi}{3} \int_{r_{min}}^{r_{max}} r^3 n(r) dr \propto [r_{max}^{4-b} - r_{min}^{4-b}] \quad (7)$$

where r_{min} and r_{max} are the minimum and maximum radii of the bubble distribution. For $b=2$, v_f is proportional to r_{max}^2 for $r_{max} \gg r_{min}$. The previous

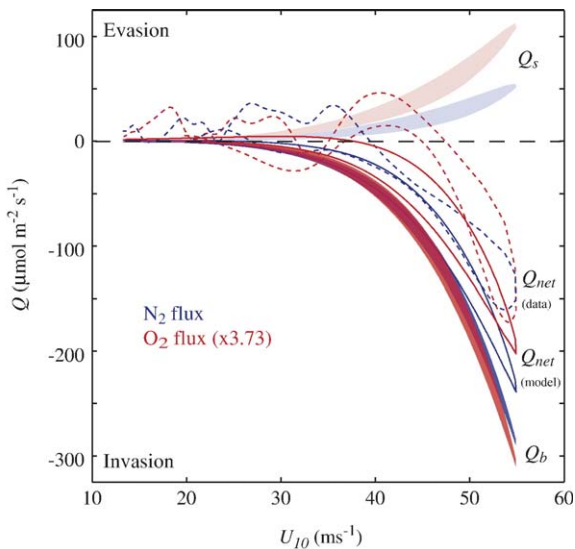


Fig. 5. Modeled air–sea gas fluxes (Q) versus wind speed at 10 m height (U_{10}), calculated using Eq. (4) for the case of $Q_i=0$. Modeled $Q_s^{O_2}$ (light red shading) and $Q_s^{N_2}$ (light blue shading) assumes $K_b = K_s = K_T/2$ and uses K_T derived from the Hurricane Frances measurements (see heavy dashed red line marked HF in Fig. 3). Modeled $Q_b^{O_2}$ (heavy red shading) and $Q_b^{N_2}$ (heavy blue shading) use the Woolf and Thorpe (1991) model, i.e., $\delta = \Delta$, $U_{O_2} = 9.0 \text{ m s}^{-1}$, and $U_{N_2} = 7.2 \text{ m s}^{-1}$. Modeled $Q_{net}^{O_2} = Q_s^{O_2} + Q_b^{O_2}$ (solid red line) can be compared to the data (dashed red line). Modeled $Q_{net}^{N_2} = Q_s^{N_2} + Q_b^{N_2}$ (solid blue line) can be compared to the data (dashed blue line). All O_2 fluxes (red lines and shading) are amplified by a factor of 3.73.

calculations shown in Fig. 1c are used for r_{\max} . The total flux of air associated with the descending bubble plume is:

$$V = wv_f \quad (8)$$

where w is the vertical downward velocity of the individual plume (see Fig. 1b). The resulting estimates of Q_i are described statistically. The mean plus two times the individual standard deviation of the Q_i estimates are derived, and assumed to represent the wind speed dependence of the most energetic plumes which are believed to contribute most of the bubble injection flux. Note that this analysis provides only the wind speed dependence of the estimate V . The absolute flux requires information on bubble number densities. Bubble flux estimates are then normalized over the observed range of wind speed according to the estimate of V_T derived from the budget-derived gas fluxes described in Section 4.7.

Given that the measurements were made during a hurricane, it is reasonable to assume a very turbulent and bubbly near surface layer from which the turbulent plumes are drawing bubble from. A reasonable choice is $b=2$, rather than $b=1$, which would be more suitable for an active breaking wave environment, or $b=4$, which would be more suitable for describing deep bubble plumes consisting of very small bubbles. Fig. 4 shows an estimate of V for the case of $b=2$ (thick green line). Also shown, for comparison, is the case for $b=4$ (thin green line). The wind speed dependence of the estimate for $b=2$ (thick green line), derived using bubble dynamics, agrees well with the wind speed dependence of the data derived Q_{BT} (heavy red and blue shading in Fig. 4). This result provides further evidence that most of the measured N_2 and O_2 fluxes at the peak of the storm were associated with complete bubble injection processes.

4.11. Applicability to CO_2 transfer under hurricane force winds

It is important to address how the model and results described above may apply to the air–sea exchange of CO_2 under hurricane force winds, because it is believed that hurricanes, on the average, remove CO_2 from the ocean (Bates et al., 1998; Bates, 2002; Perrie et al., 2004). CO_2 is much more soluble in seawater than N_2 or O_2 . Because of this, it is expected (e.g., Keeling, 1993; Woolf, 1997) that the bubble-induced supersaturation of CO_2 would be only a small fraction of that of N_2 and O_2 (i.e., δ for CO_2 would be much less than δ for N_2 or O_2). Maximum bubble induced saturations of O_2 and N_2 during Hurricane Frances

were approximately 12%, so bubble induced supersaturation of CO_2 must be significantly less than this.

One calculation related to the air–sea flux of CO_2 that is unaffected by complications in gas scaling laws follows. During the peak winds of Hurricane Frances, the total volume flux of air injected into the ocean by completely dissolving bubbles is estimated to be approximately $200 \mu\text{mol air m}^{-2} \text{ s}^{-1}$, or approximately $5 \text{ ml air m}^{-2} \text{ s}^{-1}$. If the bubbles are assumed to be 1 mm in radii (see Fig. 1a), this would represent a bubble flux into the ocean of approximately $1200 \text{ bubbles m}^{-2} \text{ s}^{-1}$. The net flux of atmospheric CO_2 into the ocean associated with these bubbles is $0.26 \text{ mmol } CO_2 \text{ m}^{-2} \text{ h}^{-1}$. This is less than 2% of the typical flux of CO_2 out of the ocean during hurricanes as estimated by Bates et al. (1998) and Perrie et al. (2004). This calculation shows that CO_2 invasion associated with complete bubble injection during hurricanes is probably insignificant compared to expected net CO_2 evasion.

Because the net N_2 and O_2 fluxes during Hurricane Frances are explainable by air–sea gas transfer rates that fall somewhere between the LM-86 and W-92 parameterizations (see Fig. 3), it is likely that WM-99 would greatly over-predict air–sea fluxes of CO_2 at extreme wind speeds (see Fig. 3, compare HF and WM-99).

5. Conclusions

Recent field measurements made during Hurricane Frances showed a new regime of gas transfer developing at $U_{10} > 35 \text{ m s}^{-1}$ in which complete bubble injection processes become important in air–sea exchange of weakly soluble gases (D'Asaro and McNeil, 2006). The conversion of the measured gas fluxes to transfer rates requires use of a bubble-mediated air–sea gas exchange model. The standard Woolf (1997) model could not reproduce the expected theoretical response to a step change in wind speed over the ocean under limiting cases. This limitation was overcome, without significantly changing the underlying physics of the model, by separating the surface flux term (Q_s) and the partial bubble dissolution flux term (Q_b) in the original equation. To expand the applicability of the adapted model to $U_{10} > 27 \text{ m s}^{-1}$, new physics was added based on the Hurricane Frances observations by adding a complete bubble injection flux term (Q_i). A new formulation of air–sea gas transfer was presented (Eq. (4)) which spans the full range of wind speed over the ocean. Fundamentally, the new model has 4 coefficients (K_s , K_b , δ , V) that represent the various physical processes occurring over low to extreme winds speeds. The

equation can be rearranged and simplified to have 3 coefficients ($K_T = K_s + K_b$, $K_b \delta S$, V). In its most simplified form, it has 2 coefficients (K_T , $V_T = K_b \delta S + V$) where for supersaturated waters the first coefficient represents all surface evasion processes and the second all subsurface supersaturating processes.

The Hurricane Frances data were analyzed using solutions to the most simplified form of the new model and empirical expressions as a function of wind speed were found for the surface and subsurface equilibration processes. The resulting estimates of air–sea gas transfer velocities for surface equilibration processes (K_T), which span $U_{10} = 14\text{--}50 \text{ m s}^{-1}$, indicate that the best estimates of K_T at hurricane force winds lie somewhere between LM-86 and W-92, and exclude WM-99 at hurricane force winds (see Section 4.5, Fig. 3, HF line). It is concluded that WM-99 would over-predict air–sea gas transfer rates at hurricane force winds.

The new model of air–sea gas exchange was calibrated using the Hurricane Frances data, and K_T was found to scale with U_{10} according to a power law with exponent 3.7 ± 1.4 . An inverse model-derived estimate of K_T (see Section 4.6) agreed with the O_2 covariance- and O_2 deficit-derived estimates (see Sections 4.3 and 4.4). A second relationship that describes bubble injection fluxes ($Q_{\text{BT}}^{\text{Air}}$, see Section 4.7) was found to scale with U_{10} according to a power law with exponent 6.35 ± 0.06 . It is concluded that the net air–sea gas exchange of weakly soluble gases, such as O_2 and N_2 , can be parameterized over the full range of oceanic wind speeds using these two relationships, K_T and $Q_{\text{BT}}^{\text{Air}}$ versus U_{10} . This conclusion is subject to the assumption that the observed fluxes were only a function of U_{10} , as discussed previously.

The model-derived estimate of Q_{BT} for both gases (see Fig. 4, heavy red and blue shading) increased at $U_{10} > 27 \text{ m s}^{-1}$, reaching a factor of up to 2.2 times that of Q_{ST} at $U_{10} = 55 \text{ m s}^{-1}$. Because $Q_{\text{BT}}/Q_{\text{ST}} > 1$ for both gases at $U_{10} > 37 \text{ m s}^{-1}$ (see Fig. 4), it is concluded that complete bubble injection is the main transfer mechanism of weakly soluble gases at $U_{10} > 37 \text{ m s}^{-1}$.

And lastly, a new formulation was presented that parameterizes complete bubble injection (Q_i) in terms of the bubble size distribution near the ocean surface and statistical descriptions of downward flowing turbulent currents emanating from the near surface bubble zone. The formulation was tested using the Hurricane Frances float data and an assumed near-surface bubble size distribution. The wind speed dependence of Q_i derived using the new formulation showed reasonable agreement with the wind speed dependence of $Q_{\text{BT}}^{\text{Air}}$. This result indicates that Q_i can ultimately be estimated directly from field measurements.

Acknowledgements

This work was supported by NSF Grants OCE 0220692 and 0220687.

References

- Asher, W.E., Karle, L.M., Higgins, B.J., Farley, P.J., Leifer, I.S., Monahan, E.C., 1996. The influence of bubble plumes on air/seawater gas transfer velocities. *Journal of Geophysical Research* 101(C), 12027–12042.
- Bates, N.R., 2002. Interannual variability in the global ocean uptake of CO_2 . *Geophysical Research Letters* 29 (5), 1059. doi:10.1029/2001GL013571.
- Bates, N.R., Knap, A.H., Michaels, A.F., 1998. Contribution of hurricanes to local and global estimates of air–sea exchanges of CO_2 . *Nature* 395, 58–61.
- Broecker, W.S., Peng, T.-H., Ostlund, G., Stuiver, M., 1985. The distribution of bomb radiocarbon in the ocean. *Journal of Geophysical Research* 99, 6953–6970.
- Clift, R., Grace, J.R., Weber, M.E., 1978. *Bubbles, Drops and Particles*. Academic Press, New York. 380 pp.
- D'Asaro, E.A., 2003. The ocean boundary layer below Hurricane Dennis. *Journal of Physical Oceanography* 33, 561–579.
- D'Asaro, E.A., 2004. Air–sea heat flux measurements from nearly neutrally buoyant floats. *Journal of Atmospheric and Oceanic Technology* 21, 1086–1094.
- D'Asaro, E.A. and McNeil, C.L., 2006. Measurements of air–sea gas exchange at extreme wind speeds measured by autonomous oceanographic floats. *Journal Marine Systems*, this edition.
- Garcia, H.E., Gordon, L.I., 1992. Oxygen solubility in seawater: better fitting equations. *Limnology and Oceanography* 37 (6), 1307–1312.
- Hamme, R.C., Emerson, S.R., 2002. Mechanisms controlling the global oceanic distribution of the inert gases argon, nitrogen, and neon. *Geophysical Research Letters* 29 (23), 1–4.
- Hamme, R.C., Emerson, S.R., 2004. The solubility of neon, nitrogen, and argon in distilled water and seawater. *Deep-Sea Research. Part 1. Oceanographic Research Papers* 51 (11), 1517–1528.
- Keeling, R.F., 1993. On the role of large bubbles in air–sea gas exchange and supersaturation in the ocean. *Journal of Marine Research* 51, 237–271.
- Liss, P.S., Merlivat, L., 1986. Air–sea exchange rates: introduction and synthesis. In: Buat-Menard, P. (Ed.), *The Role of Air–sea Exchange in Geochemical Cycling*. Reidel, Dordrecht, pp. 113–127.
- McNeil, C.L., D'Asaro, E.A., Johnson, B.D., Horn, M., in press. A gas tension device with response times of minutes. *Journal of Atmospheric and Oceanic Technology*. doi:10.1175/JTECH1974.1.
- Nightingale, P.D., Malin, G., Law, C.S., Watson, A.J., Liss, P.S., Liddicoat, M.I., Boutin, L., Upstill-Goddard, R.C., 2000. In-situ evaluation of air–sea gas exchange parameterizations using novel conservative and volatile tracers. *Global Biogeochemical Cycles* 14, 373–387.
- Perrie, W., Zhang, W., Ren, X., Long, Z., Hare, J., 2004. The role of midlatitude storms on air–sea exchange of CO_2 . *Geophysical Research Letters* 31, L09306. doi:10.1029/2003GL019212.
- Powell, M.D., Houston, S.H., Amat Jr., L.R., Morisseau-Leroy, N., 1998. The HRD real-time hurricane wind analysis system. *Journal of Wind Engineering and Industrial Aerodynamics* 53–64.
- Spitzer, W.S., Jenkins, W.J., 1989. Rates of vertical mixing, gas exchange and new production: estimates from seasonal gas cycles in the upper ocean near Bermuda. *Journal of Marine Research* 47, 169–196.

- Wanninkhof, R., 1992. Relationship between gas exchange and wind speed over the ocean. *Journal of Geophysical Research* 97, 7373–7381.
- Wanninkhof, R., McGillis, W.R., 1999. A cubic relationship between air–sea CO₂ exchange and windspeed. *Geophysical Research Letters* 26, 1889–1892.
- Woolf, D.K., 1997. Bubbles and their role in gas exchange. In: Liss, P.S., Duce, R.A. (Eds.), *The Sea Surface and Global Change*. Cambridge University Press, Cambridge, UK, pp. 173–205.
- Woolf, D.K., Thorpe, S.A., 1991. Bubbles and the air–sea exchange of gases in near-saturation conditions. *Journal of Marine Research* 49, 435–466.